CR-184028

May 22, 1990

Interim Report

SEPAC DATA ANALYSIS IN SUPPORT OF THE ENVIRONMENTAL INTERACTION PROGRAM

NASA Contract NAS8-32488; Task 4

Southwest Research Institute Project No. 15-4865-009

Chin S. Lin

Project Manager

(NASA-CR-184028) SEPAC DATA ANALYSIS IN SUPPORT OF THE ENVIRONMENTAL INTERACTION PROGRAM Interim Report (Southwest Research Inst.) 51 p

N91-13807

CSCL 13B

Unclas

G3/45 0309740

TABLE OF CONTENTS

1. Introduction

This interim report describes the work completed in the last 12 months. It contains two parts; the first part describes the results from modeling spacecraft charging potential during electron beam injections into a background of neutral gas and plasma, whereas the second part describes the simulation results about the radial expansion of an electron beam injected into space plasma. We are currently revising both articles for submitting them to journals for publication. The first paper has been presented at the Spacecraft Charging Technology Conference at Montreal in August 1989.

Part 1

PIC Code Modeling of Spacecraft Charging Potential During Electron Beam Injection Into a Background of Neutral Gas and Plasma

J. K. Koga and C. S. Lin

Department of Space Sciences

Southwest Research Institute

San Antonio, Texas 78284

R. M. Winglee

Dept. of Astrophysical, Planetary and Atmospheric Sciences

Univ. of Colorado, Boulder

Abstract

Injections of nonrelativistic electron beams from an isolated equipotential conductor into a uniform background of plasma and neutral gas have been simulated using a two-dimensional electrostatic particle code. The ionization effects on spacecraft charging are examined by including interactions of electrons with neutral gas. The simulations show that the conductor charging potential decreases with increasing neutral background density due to the production of secondary electrons near the conductor surface. In the spacecraft wake, the background electrons accelerated towards the charged spacecraft produce an enhancement of secondary electrons and ions. Simulations run for longer times indicate that the spacecraft potential is further reduced and short wavelength beam-plasma oscillations appear. The results are applied to explain the spacecraft charging potential measured during the SEPAC experiments from Spacelab 1.

INTRODUCTION

Nonrelativistic electron beams have been injected from rockets and the Space shuttle to study beam propagation, instabilities and other space plasma problems in the ionosphere [1]. Several experimental and theoretical studies have focused on the spacecraft charging phenomenon during the electron beam injection [2]-[5]. At low beam current, Spacelab 2 experiments indicated that electron beams can propagate away after beam degradation and expansion [6]. However, at high beam current, Space Experiments with Particle Accelerators (SEPAC) during the Spacelab 1 mission indicated that the electron beam injection had charged the spacecraft to a potential as high as the beam energy, which was 5 keV [2]. Neutralization of spacecraft charging is therefore important for allowing the injected electron beam to propagate away. SEPAC experiments have suggested that a large conductor surface area for collecting currents from ambient plasma will reduce spacecraft charging.

It is also well known that neutral gas ionization by the electron beam can help neutralize spacecraft charging. At altitudes below 160 km where neutral densities are high, electron beam experiments on sounding rockets indicate that payload charging was reduced and sometimes even completely neutralized [7]. Plasma enhancement associated with Beam Plasma Discharge (BPD) [8] is believed to be responsible for the charging neutralization of sounding rockets. During SEPAC electron beam experiments Marshall et al. [5] reported anomalous features in the measurement of return current by Langmuir probe when an energetic electron beam was injected into a dense cloud of Argon gas. They interpreted the anomalous current signature as due to secondary electron fluxes escaping from the spacecraft and the formation of a double layer structure. In all cases of SEPAC experiments the spacecraft potential charged by an

electron beam was small relative to the beam energy when neutral gas is present.

The purpose of this paper is to model the effects of neutral gas ionization on spacecraft charging due to electron beam injection. We use a two-dimensional electrostatic particle code to simulate the injection of electron beams from an isolated equipotential conductor into uniform background of plasma and neutral gas. In this preliminary study we examine how the spacecraft charging potential varies with neutral density.

Several simulation studies have examined the general relationship between the spacecraft charging and the electron beam injection in the ionosphere [9]-[13]. These studies show that the positively charged spacecraft attracts the ambient and beam electrons to neutralize the charging partially. Some electrons in the beam head, however, are accelerated forward and propagate away. Winglee and Prichett [14] indicate that the spacecraft charging potential varies with the the injection angle of the beam relative to the magnetic field lines. Furthermore, the spacecraft charging potential exceeds the beam energy when the spacecraft surface is small relative to the return current region. Examining the surface effects of the spacecraft, Lin and Koga [15] model the production of backscattered and secondary electrons generated at the conductor surface. Their simulations indicate the spacecraft potential increases with the reflection coefficient, which is defined as the ratio of electrons reflected from the spacecraft surface.

Simulations of the interactions of an electron beam with neutral gas are difficult because they require a large memory and a long computation time. In this conference Winglee [16] examines the effects of a neutral gas cloud in the vicinity of the spacecraft on the beam propagation and charging. In this study, we consider a uniform neutral gas background.

Furthermore, we assume that the electrons are scattered isotropically by neutral gas whereas Winglee [16] emphasizes small angle scattering.

SIMULATION MODEL

To study electron beam injection from a conductor, we modified a 2-D particle-in-cell code DARWIN, which was originally developed at Los Alamos National Laboratory [17]. Here we present the simulation results in the electrostatic limit. We improve the modeling by considering (1) the injection of an electron beam from a finite isolated conductor and (2) collisional ionization of neutrals by beam, background, and secondary electrons. Figure 1 illustrates the simulation geometry.

We model the spacecraft as a rectangular conductor within the simulation system, which injects electrons from the spacecraft surface every timestep. The number of injected electrons per time step per cell is $N_c(n_b/n_c)v_b\Delta t$ where N_c is the number of ambient electrons per cell, Δt is the simulation time step, and n_b/n_c is the ratio of the beam density to background density. We assign the positions of the injected particles as $x = Rv_b\Delta t$ where x is the distance from the conductor surface, v_b is the injection velocity, and R is a random number between 0 and 1 for each injected particle. In the y direction we randomly distribute the injected particles across the beam. Therefore the injected particles fill in the fan between $x = 0$ and $x = v_b\Delta t$. In this study we assume that the spacecraft surface absorbs all particles striking the surface and accumulates the charge.

We use the capacity matrix method [18] to treat the spacecraft surface as a finite isolated equipotential conductor in a background plasma. The capacity matrix C_{ij} relates the charge,

q_i, on each grid point on the spacecraft to the corresponding potential Φ_j through

$$q_i = \sum_j C_{ij}\Phi_j \tag{1}$$

where the sum j is over every grid point on the spacecraft. The capacity matrix is obtained by placing a unit charge on one point of the spacecraft surface with all other points zero and then solving for the potential. The values of the potential at each point on the spacecraft represent one column in the inverse capacity matrix $A = C^{-1}$. Repeating the process for each node then generates the full inverse matrix. The capacity matrix is obtained from the inverse of this matrix. This process is carried out only once at the beginning of the program. During the program the code first solves Poisson's equation for the electric potential Φ_0 with the charge evenly distributed on the spacecraft surface. Second, it uses the capacity matrix of the conductor to redistribute the charge and maintain the spacecraft surface at an equipotential using the formulae:

$$\Delta q_i = \sum_j C_{ij}(\Phi_{eq} - \Phi_{0j}) \tag{2}$$

$$\Phi_{eq} = \sum_{ij} C_{ij}\Phi_{0j} / \sum_{ij} C_{ij} \tag{3}$$

where Δq_i is the charge that is added to each grid point on the spacecraft. Using the redistributed charge density, the code again solves Poisson's equation for the electric potential of the spacecraft.

We use a periodic boundary condition for the lower boundary at $y = 0$ and the upper boundary at $y = L_y$ where L_y is the simulation length in the y direction. The electrostatic potential at $x = 0$, $\phi(x = 0, y)$, is constant. We assume the potential is zero at the right

boundary at $x = L_x$ where L_x is the simulation length in the x direction. The right boundary condition approximates the potential at the infinity.

In our model we include the interaction of beam, background, and secondary electrons with neutral particles following the approach of Machida and Goertz [19]. The neutral particles are assumed uniformly distributed through the system. To allow the simulations to run for much longer times, a very high density neutral region is added at the right hand side of the simulation box. Beam electrons entering into this region are slowed down enough by collisions so that they are not reflected back into the simulation box with high velocities. All neutral particles are assumed to have a Maxwellian velocity distribution.

The ionization rate of the neutral particles is determined from the incoming electron velocity, the neutral density, and the ionization collisional cross section. The ionization collisional cross section varies with the incoming electron energy according to a fit to an experimental curve for O_2 [20]. We first calculate the ionization cross section based on the particle's energy and then calculate the average collisional ionization frequency from the cross section. Assuming that the event occurrence follows an exponential probability distribution, we assign a probability P_i of collisional ionization to the beam electrons at each time step from the collision frequency. The probability is then compared with a uniform set of random numbers R_i between 0 and 1. A collision occurs if $P_i > R_i$.

A fixed ionization energy is subtracted from the incident particle energies after the collision. The velocity vectors of the electrons and ions after the collision are calculated from momentum conservation, energy conservation, and the assumption that the collisions are head on. Random directional angles are assigned to the particles after the collision. Other

collisional processes can be handled in the same way as ionization collisions by using the appropriate collision frequency.

Background plasma ions and electrons are initialized uniformly in the system with a uniform magnetic field in the x direction. Both the background ions and electrons have Maxwellian velocity distributions with the same temperature, $T_e = T_i$ where T_e and T_i are the electron and ion temperatures, respectively. At the right and left boundary, the code specularly reflects all particles.

SIMULATION RESULTS

The simulation uses a $512\Delta \times 128\Delta$ grid in the x and y directions respectively. The spacecraft is represented by a rectangular box centered on $x = 102\Delta$ and $y = 64\Delta$ with size $4\Delta \times 32\Delta$ in the x and y directions respectively. The grid size, Δ, equals the Debye length of the ambient electrons defined as $\lambda_d = a_c/\omega_{pe}$ where $a_c = (2T_e/m_e)^{1/2}$ is the thermal velocity of the ambient electrons and ω_{pe} is the ambient electron plasma frequency. In the simulations $a_c = 0.001c$ where c is the speed of light, a unit of the simulation. We choose the secondary ion to electron mass ratio to be 1836. We assume the electron gyrofrequency Ω_{ce} to be $0.5\omega_{pe}$, which is close to the ionospheric value of $0.3\omega_{pe}$. The simulations use a time step $\Delta t = 0.05\omega_{pe}^{-1}$ and 131,072 particles for the background plasma. The electron beam has a width of 2Δ, an injection velocity of $v_b = 10a_c$, and zero thermal velocity. In this study, the density ratio n_b/n_o is 10 where n_b and n_o are the densities of the electron beam and the ambient electrons, respectively. In SEPAC experiments this ratio was approximately 100 for a 100 mA beam.

Figures 2 and 3 present the modeling results of an electron beam with no neutral background. The phase space plot at $\omega_{pe}t = 30$ indicates that the stagnation point of the injected electron beam is very close to the conductor surface (Figure 2a). Also it shows that beam electrons at the front are accelerated to velocities above the initial beam velocity, due to the buildup of beam electrons behind the front of the beam head. Figure 2b, the configuration space plot, shows that the electron beam expands radially due to mutual repulsion. The beam expands a maximum width of 40Δ near the spacecraft surface. Figure 3 shows the time variation of the spacecraft potential for the duration of the simulation. The oscillations in the potential correspond to the background plasma frequency. Note that after the quick rise in the potential to 75% of the beam energy the average potential is approximately 70% of the beam energy.

Figures 4-6 present results of an electron beam injected into a uniform background of neutral particles. The neutral number density is 10^{14} cm^{-3} corresponding to a pressure of 10^{-4} Torr at room temperature. The beam phase space plot at $\omega_{pe}t = 30$ in Figure 4a shows that the stagnation point of the beam is farther away from the spacecraft than the case with no neutral background. The beam electrons travel farther before being substantially slowed down because secondary electrons created from ionization of neutrals impinge on the spacecraft and reduce the charge. The configuration space plot in Figure 4b shows beam expansion similar to the case with no neutral background at $\omega_{pe}t = 30$. The maximum width remains at about 40Δ. The phase space plots of secondary electrons are shown in Figure 5. Figure 5a indicates that some secondary electrons near the spacecraft have been scattered to energies comparable to the beam energy. Most secondary electrons are produced near the

spacecraft surface while some are produced in the wake region of the spacecraft, as shown in the configuration space plot (Figure 5b). Secondary electrons are produced in the wake as background electrons are accelerated towards the charged spacecraft and ionize neutral particles. Figure 6 presents spacecraft potential as a function of time. The oscillations in the potential again correspond to the background plasma frequency. After a quick rise in the potential to 75% of the beam energy, the average potential energy of the spacecraft drops to about 40% of the beam energy. This reduction in the potential is caused by the increase in plasma density around the spacecraft from ionizations. Figure 7 shows spacecraft potential at $\omega_{pe}t = 30$ for various values of background neutral density. This figure indicates that increasing the neutral density reduces the spacecraft potential. Two factors contribute to the reduction in the charging potential. First, higher neutral densities result in more collisional ionizations and therefore a larger number of secondary electrons to neutralize the spacecraft. Second, higher neutral densities result in shorter mean free paths for the beam electrons. Scattering of the beam electrons occurs closer to the spacecraft and fewer beam electrons escape. In the highest neutral density case of 10^{15} cm^{-3}, the potential is reduced to 10% of the beam energy. Also the spacecraft potential oscillations increase in frequency due to the large increase in the plasma density near the spacecraft.

Figure 8 shows phase space plots of beam and secondary electrons from a long simulation run, $\omega_{pe}t = 60$. The neutral density is 10^{14} cm^{-3}, the same as in Figures 4–6. At $\omega_{pe}t = 60$, many beam electrons have been scattered by collisions to lower velocities (Figure 8a). Particles at the beam front no longer travel at velocities comparable to the initial beam velocity. Note that newly injected beam electrons are travelling longer distances at nearly their initial

injection velocity. They set up short wavelength beam-plasma oscillations which are apparent in the phase space plot. Figure 8b indicates that the secondary electrons are accelerated to velocities compararble to the beam velocity within the beam-plasma oscillation regions. These secondary electrons can be accelerated to the point where they contribute significantly to the collisional ionizations. A history of the spacecraft potential (Figure 9) shows that the potential is about 40% of the beam energy at $\omega_{pe}t = 30$ and is reduced to 25% of the beam energy at $\omega_{pe}t = 60$. Running the simulation for a longer time results in more secondary electrons produced near the spacecraft and also gives secondary electrons generated farther away from the spacecraft the time to respond to the positively charged spacecraft.

DISCUSSION

We have simulated the injection of a nonrelativistic electron beam from a finite conductor with a beam density much larger than the ambient density, $n_b/n_o = 10$, and have incorporated secondary electron and ion production due to collisional ionizations. The simulation results suggest that the uniform neutral background reduces the amount of spacecraft charging. Collisional ionization of the neutral particles by beam electrons results in an increase of secondary electrons. These secondary electrons help neutralize the spacecraft. The positively charged spacecraft accelerates background electrons to velocities high enough for them to ionize neutral particles, producing secondary electrons and ions in the wake region of the spacecraft. Another interesting result is that the stagnation point of the electron beam moves farther away from the spacecraft. As the spacecraft potential reduces, the beam electrons are able to travel longer distances before being stopped.

The simulations reported here appear because of limitation in computer time. The simulation runs for longer time periods indicate that charging is further reduced at later time, allowing newly injected beam electrons to leave the spacecraft region with nearly their initial velocities. These electrons set up short wavelength beam-plasma oscillations which accelerate secondary electrons to velocities close to the beam velocity.

In the future we plan to include effects from other collisional processes such as elastic scattering, charge exchange, photoionization, and ion elastic collisions. Since the current collision scheme assumes head on hard-sphere collisions, high velocity beam electrons can be scattered to large angles. Therefore, we plan to improve the collision model to include quantum mechanical effects. Another goal is to run the simulations much longer to determine if Beam Plasma Discharge can be observed.

ACKNOWLEDGMENT

The work was supported by NASA contract NAGW–1231 and by NASA Lewis Research Center through contract NAS-32488.

REFERENCES

[1] B. Grandal, "Artificial particle beams in space plasma studies", Plenum, New York, 1982.

[2] S. Sasaki, N. Kawashima, K. Kuriki, M. Yanagisawa, and T. Obayashi, "Vehicle charging observed in SEPAC Spacelab-1 experiment", *J. Spacecr Rockets*, vol. 23, no. 2, p. 129, 1986.

[3] S. Sasaki, N. Kawashima, K. Kuriki, M. Yanagisawa, T. Obayashi, W. T. Roberts, D. L. Reasoner, P. R. Williamson, P. M. Banks, W. W. L. Taylor, K. Akai, and J. L. Burch, "Neutralization of beam-emitting spacecraft by plasma injection", *J. Spacecr Rockets*, vol. 24, no. 3, p. 227,1987.

[4] I. Katz, A. Jongeward, D. E. Parks, D. L. Reasoner, and C. K. Purvis, "Energy broadening due to space-charge oscillations in high current electron beams", *Geophys. Res. Lett.*, vol. 13, no. 1, p. 64, 1986.

[5] J. A. Marshall, C. S. Lin, J. L. Burch, T. Obayashi, C. Beghin, "Spacelab 1 experiments on interactions of an energetic electron beam with neutral gas", *J. Spacecr Rockets*, vol. 25, no. 5, p. 361, 1988.

[6] D. A. Gurnett, W. S. Kurth, J. T. Steinberg, P. M. Banks, R. I. Bush, and W. J. Raitt, "Whistler-mode radiation from the Spacelab-2 electron beam", *Geophys. Res. Lett.*, vol. 13, no. 3, p. 225, 1986.

[7] E. P. Szuszczewicz, *J. Atm. Terr. Phys.*, vol. 47, p 1189, 1985.

[8] K. Papdopoulos and E. P. Szuszczewicz, "Current Understanding and issues on electron beam injection in space", *Adv. Sapce Res.*, vol. 8, no. 1, p. 101, 1989.

[9] Y. Omura, and H. Matsumoto, "Computer simulations of beam injection experiments for SEPAC/Spacelab 1 mission", *Radio Sci.*, vol. 19, no. 2, p. 496, 1984.

[10] P. L. Pritchett, and R. M. Winglee, "The plasma environment during particle beam injection into space plasmas, 1, electron beams", *J. Geophys. Res.*, vol. 92, no. A7, p. 7673, 1987.

[11] R. M. Winglee, and P. L. Pritchett, "Space charge effects during the injection of dense electron beams into space plasmas", *J. Geophys. Res.*, vol. 92, no. A6, p. 6114, 1987.

[12] H. Okuda, and J. R. Kan, "Injection of an electron beam into a plasma and spacecraft charging", *Phys. Fluids*, vol. 30, No. 1, p. 209, 1987.

[13] H. Okuda, and J. Berchem, "Injection and Propagation of a nonrelativistic electron beam and spacecraft charging", *J. Geophys. Res.*, vol. 93, no. A1, p. 175, 1988.

[14] R. M. Winglee, and P. L. Pritchett, "Comparative study of cross-field and field-aligned electrons beams in active experiments", *J. Geophys. Res.*, vol. 93, no. A6, p. 5823, 1988.

[15] C. S. Lin and J. K. Koga, "Spacecraft charging potential during electron-beam injections into space plasmas", *IEEE Trans. Plasma Sci.*, vol. 17, no. 2, p. 205, 1989.

[16] R. M. Winglee, "Spacecraft charging during electron beam injection and turnoff", in Spacecraft Charging Technology Conference proceedings, Monterey, California, 1989.

[17] C. W. Nelson and H. R. Lewis, "Particle simulation techniques in the nonradiative limit", *Methods Comput. Phys.* vol. 16, p. 367, 1976.

[18] R. W. Hockney and J. W. Eastwood, "Computer simulation using particles", McGraw-Hill, New York, 1981.

[19] S. Machida and C. K. Goertz, "The electromagnetic effect on the critical ionization velocity process", *J. Geophys. Res.*, vol. 93, no. A10, p. 11495, 1988.

[20] P. M. Banks and G. Kockarts,"Aeronomy", Academic Press, New York, 1973.

FIGURE CAPTIONS

Fig. 1. Simulation configuration.

Fig. 2. Results of simulation for $n_b/n_o = 10$ and $v_b/a_c = 10$ at $\omega_{pe}t = 30$. (a) The beam electron phase space in the x - v_x plane and (b) the positions of beam electrons in the x - y plane. The position is normalized by the Debye length and the velocity is normalized the beam velocity.

Fig. 3. Time history of the conductor potential, ϕ_o, normalized to the beam energy E_b. For this simulation, $n_b/n_o = 10$ and $v_b/a_c = 10$.

Fig. 4. Results of simulation with a uniform neutral background for $n_b/n_o = 10$ and $v_b/a_c = 10$ at $\omega_{pe}t = 30$. (a) The beam electron phase space in the x - v_x plane and (b) the positions of beam electrons in the x - y plane.

Fig. 5. Results of simulation with a uniform neutral background (a) The secondary electron phase space in the x - v_x plane and (b) the positions of secondary electrons in the x - y plane.

Fig. 6. Time history of the conductor potential, ϕ_o, normalized to the beam energy E_b.

Fig. 7. Spacecraft potential versus neutral density.

Fig. 8. Results of simulation with a uniform neutral background at $\omega_{pe}t = 60$. (a) The beam electron phase space in the x - v_x plane and (b) the secondary electrons in the x - v_x plane.

Fig. 9. Time history of the conductor potential, ϕ_o, for $\omega_{pe}t = 60$.

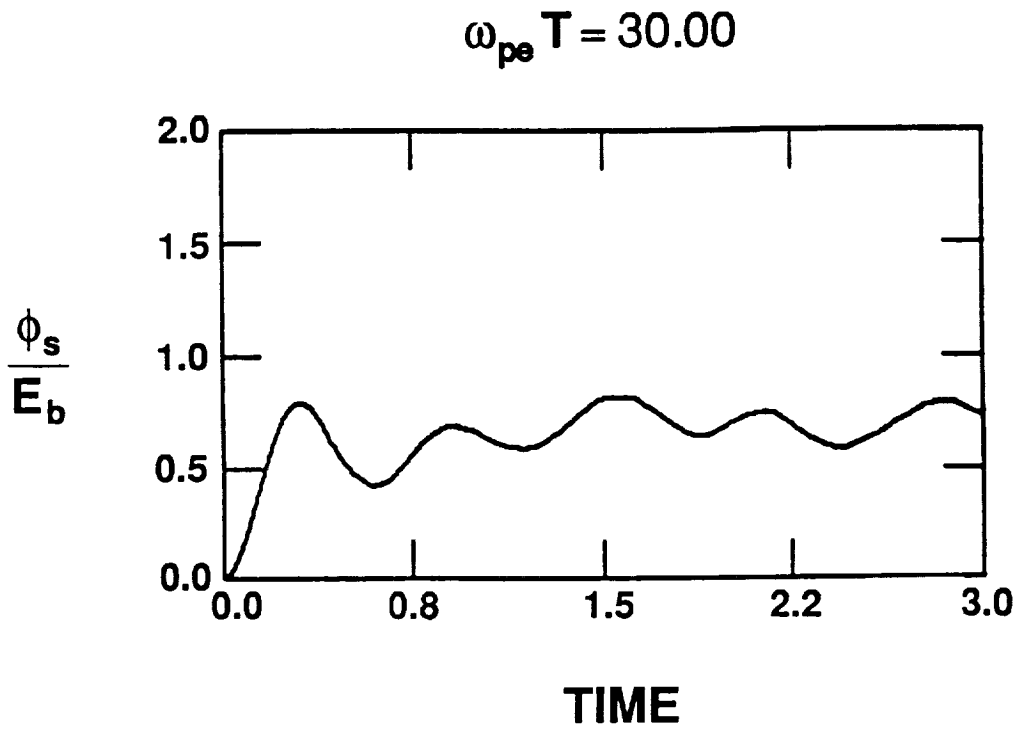

Figure 1

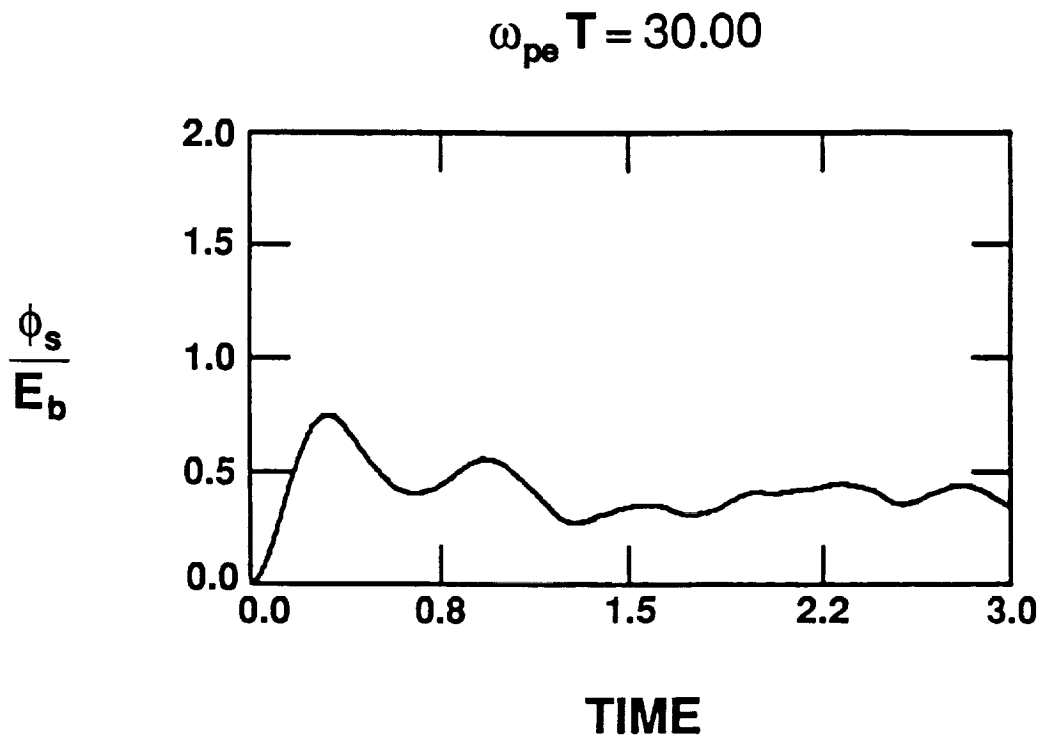

Figure 2

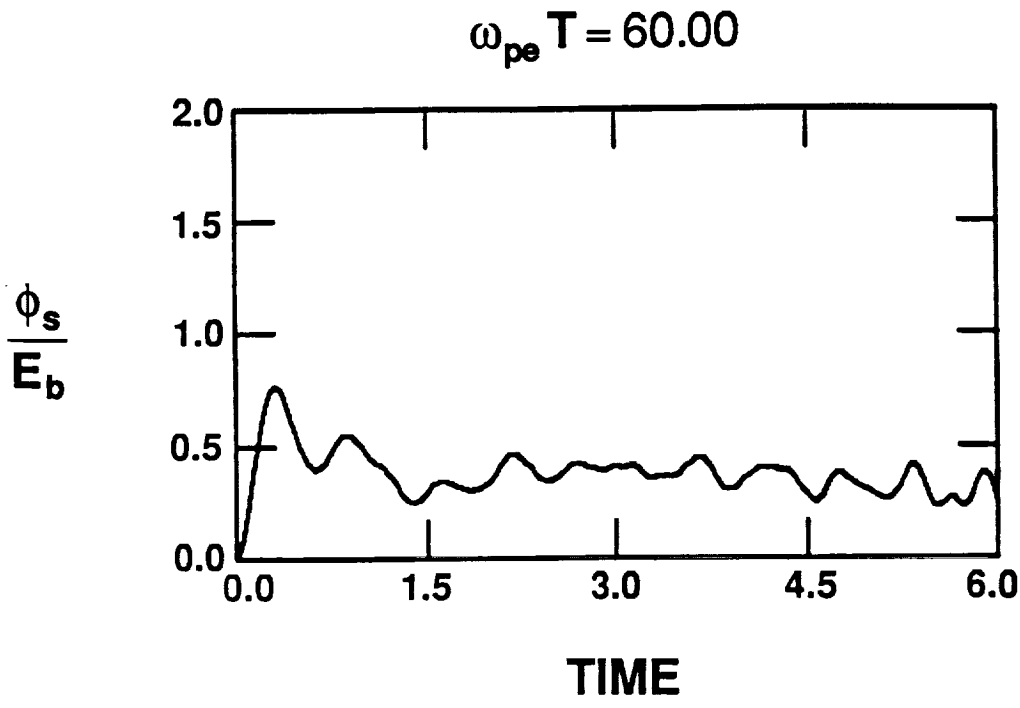

Figure 3

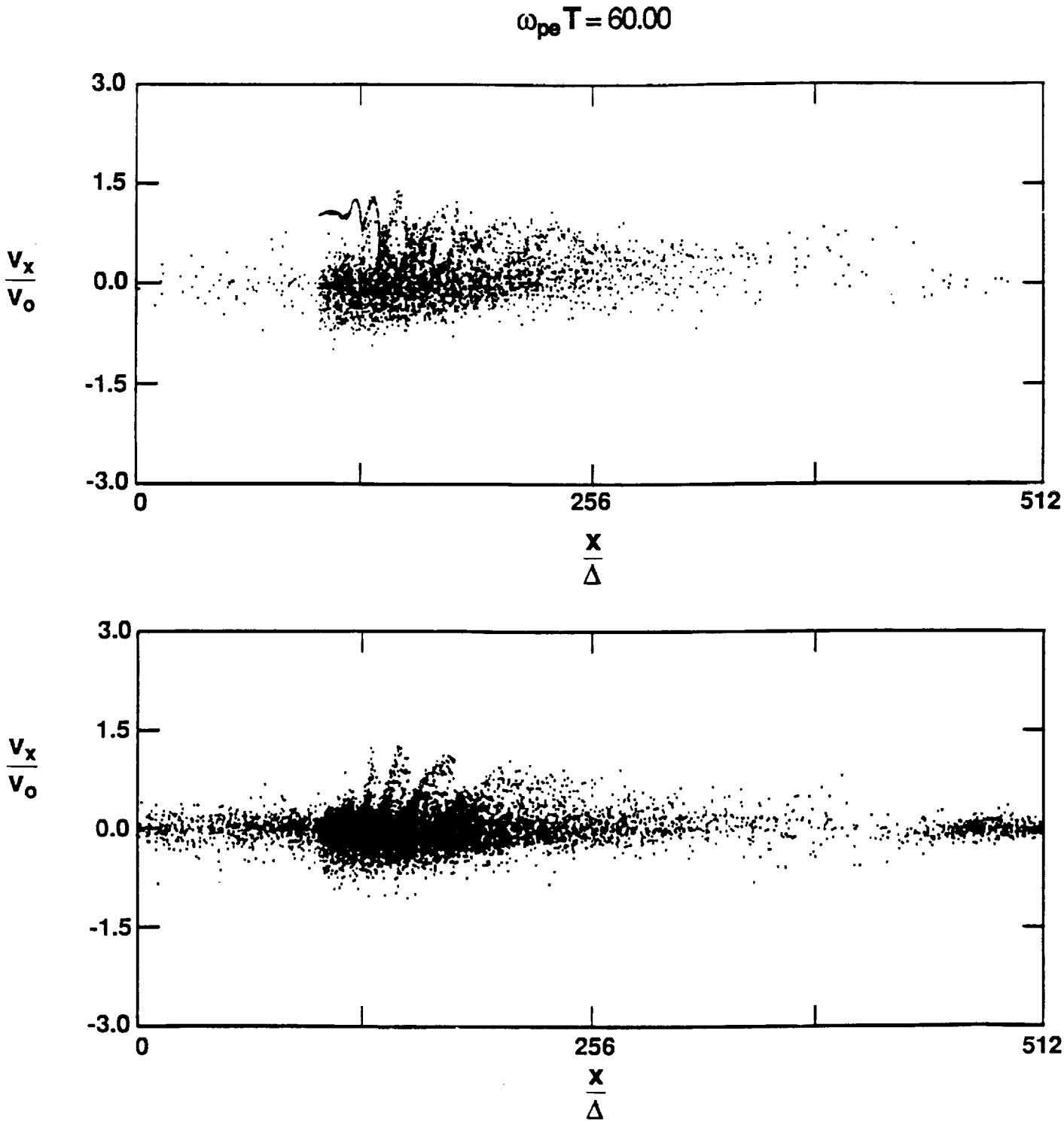
$\omega_{pe}T = 60.00$
3.0
1.5
0.0
-1.5
-3.0
$\frac{V_x}{V_o}$
0
256
512
$\frac{x}{\Delta}$
3.0
1.5
0.0
-1.5
-3.0
$\frac{V_x}{V_o}$
0
256
512
$\frac{x}{\Delta}$

Figure 4

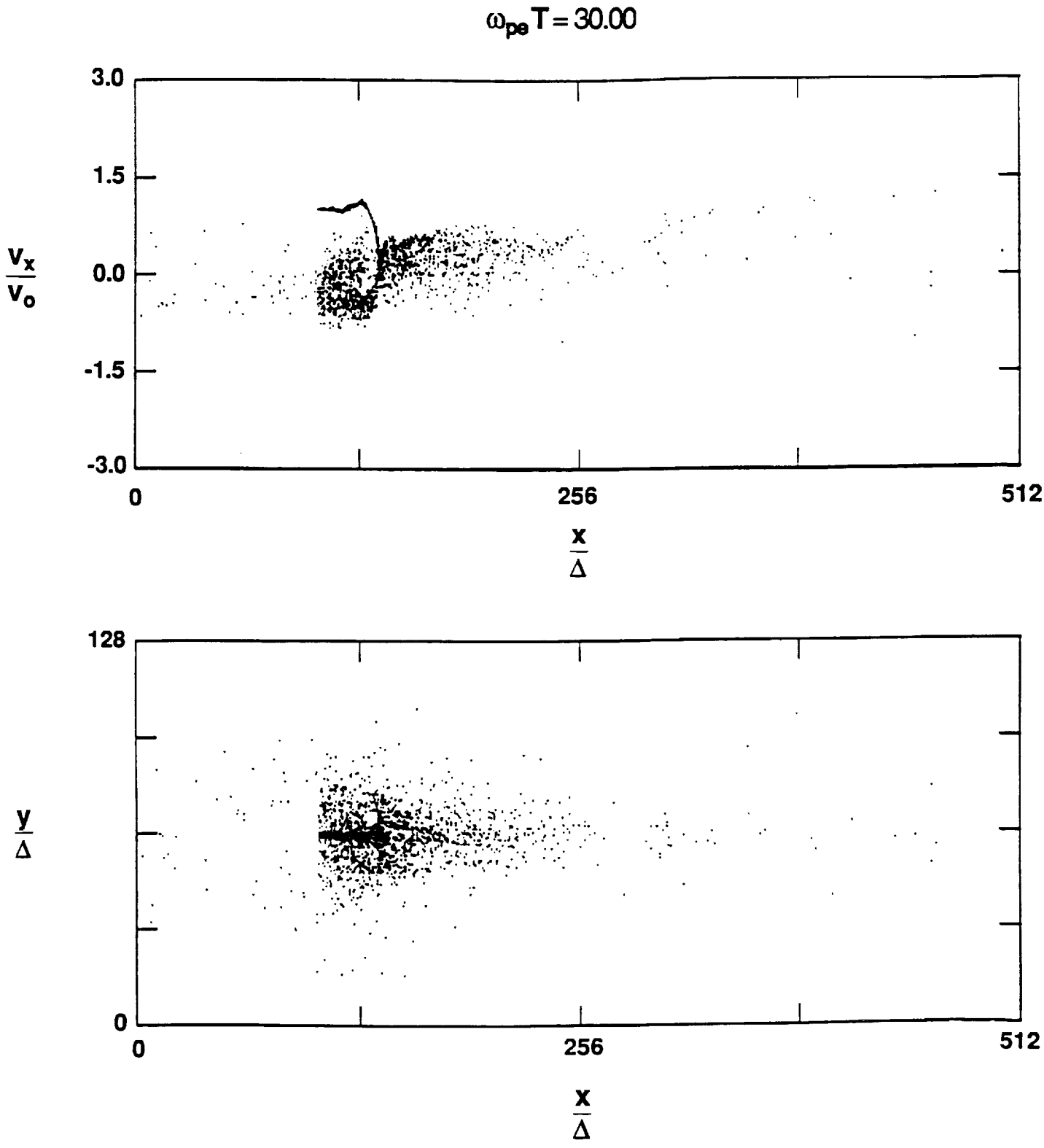
$\omega_{pe}T = 30.00$
3.0
1.5
0.0
-1.5
-3.0
$\frac{v_x}{v_o}$
0
256
512
$\frac{x}{\Delta}$
128
0
$\frac{y}{\Delta}$
0
256
512
$\frac{x}{\Delta}$

Figure 5

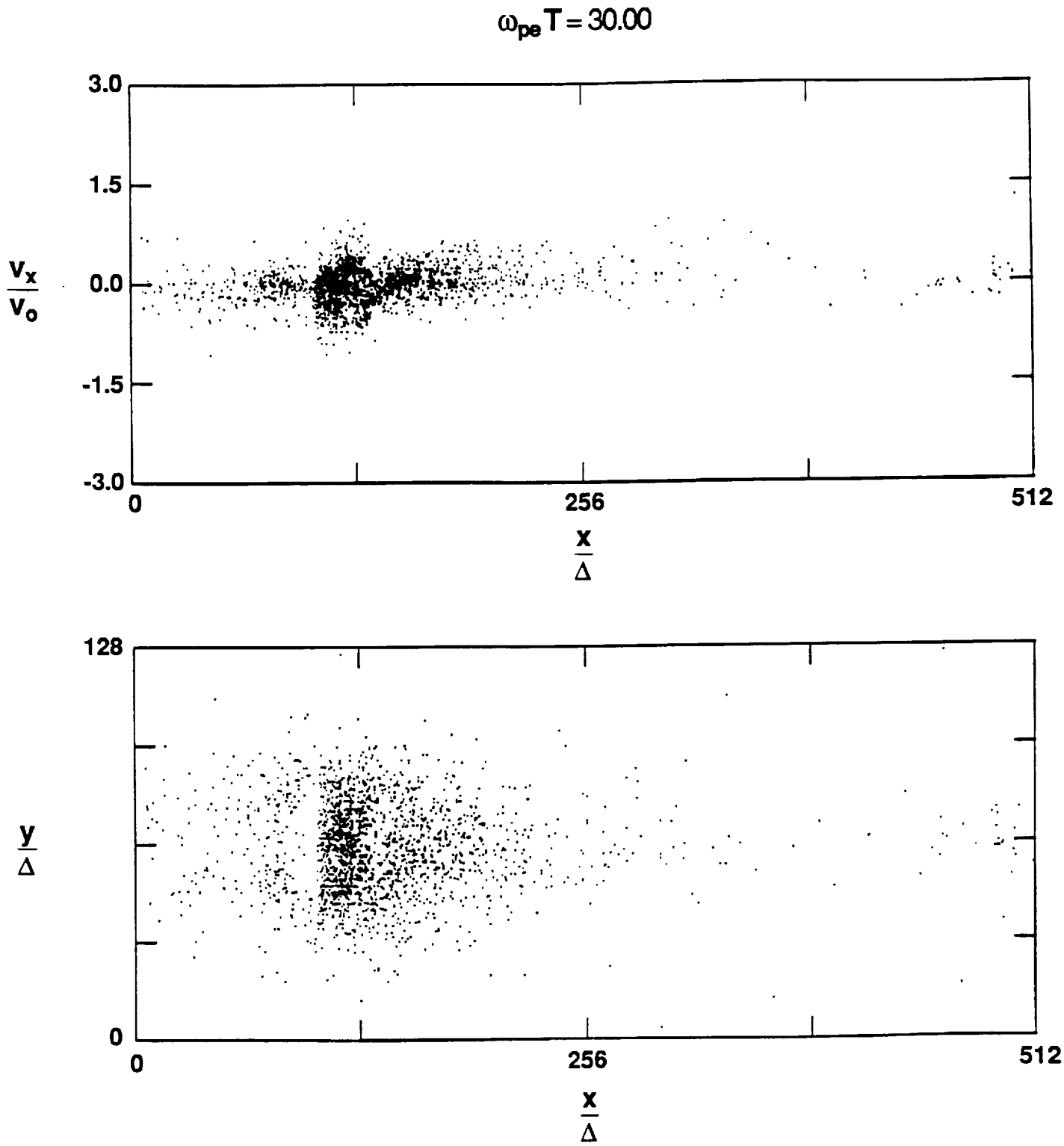
$\omega_{pe}T = 30.00$
3.0
1.5
0.0
-1.5
-3.0
$\frac{v_x}{v_o}$
0
256
512
$\frac{x}{\Delta}$
128
0
$\frac{y}{\Delta}$
0
256
512
$\frac{x}{\Delta}$

Figure 6

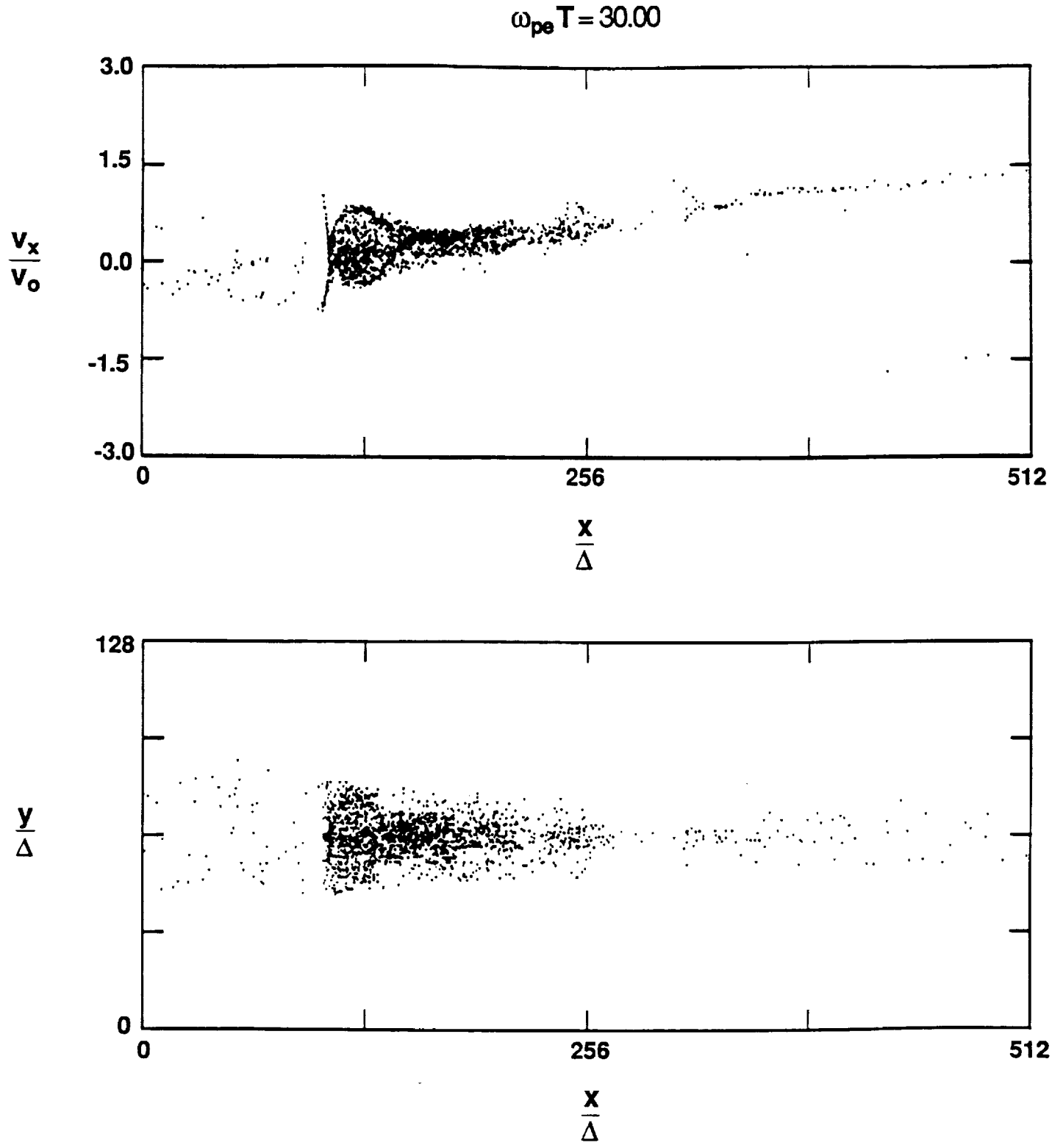
$\omega_{pe}T = 30.00$
3.0
1.5
0.0
-1.5
-3.0
$\frac{v_x}{v_o}$
0
256
512
$\frac{x}{\Delta}$
128
0
$\frac{y}{\Delta}$
0
256
512
$\frac{x}{\Delta}$

Figure 7

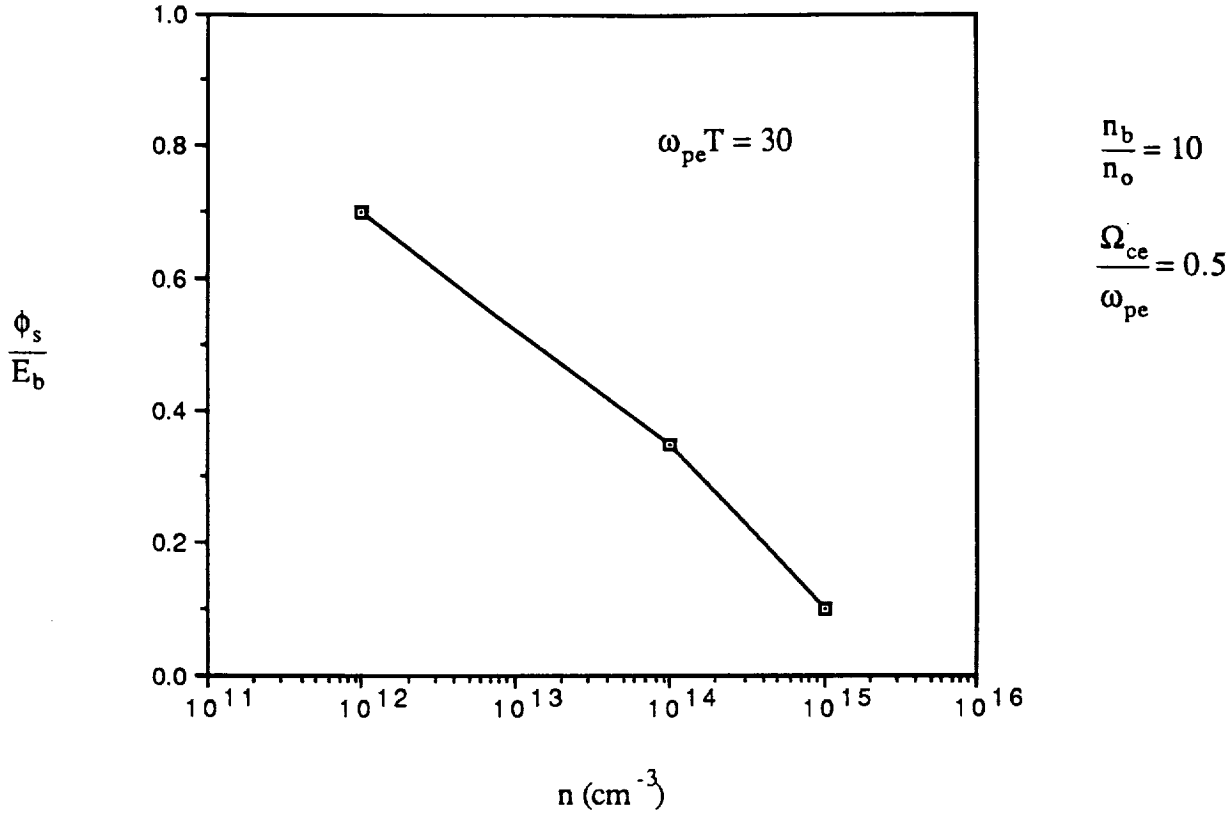
1.0
0.8
0.6
0.4
0.2
0.0
$\omega_{pe}T = 30$
$\frac{n_b}{n_o} = 10$
$\frac{\Omega_{ce}}{\omega_{pe}} = 0.5$
$\frac{\phi_s}{E_b}$
10^{11}
10^{12}
10^{13}
10^{14}
10^{15}
10^{16}
n (cm^{-3})

Figure 8

Part 2

Simulation of Radial Expansion of an Electron Beam Injected into a Background Plasma

J. Koga and C. S. Lin

Department of Space Sciences

Southwest Research Institute

San Antonio, Texas 78284

Abstract

A two-dimensional electrostatic particle code has been used to study the beam radial expansion of a nonrelativistic electron beam injected from an isolated equipotential conductor into a background plasma. The simulations indicate that the beam radius is generally proportional to the beam electron gyroradius when the conductor is charged to a large potential. The simulations also suggest that the charge buildup at the beam stagnation point causes the beam radial expansion. From a survey of the simulation results, it is found that the ratio of the beam radius to the beam electron gyroradius increases with the square root of beam density and decreases inversely with beam injection velocity. This dependence is explained in terms of the ratio of the beam electron Debye length to the ambient electron Debye length. These results are most applicable to the SEPAC electron beam injection experiments from Spacelab 1, where high charging potential was observed.

INTRODUCTION

Over the past 10 years, nonrelativistic electron beams have been injected into a background plasma and neutral gas to study beam propagation, instabilities, spacecraft charging, and other space plasma problems in the ionosphere [1–5]. Some experiments specifically examined the radial expansion characteristics of the beam [2–3], indicating that the beam expansion characteristics depend in a complex way on beam propagation angle and spacecraft charging. Many simulation studies have studied the general relationship between spacecraft charging and the electron beam injection in the ionosphere [6–12]. However, few have focused on understanding the radial expansion phenomenon. The purpose of this paper is to report our simulation study on the beam radial expansion.

In the Vehicle Charging and Potential (VCAP) experiment on the Space Shuttle Orbiter mission, the STS-3 camera imaged a narrow collimation of an electron beam fired transverse to the magnetic field for 0.3 m before the light emission of the electron beam abruptly decreased [2–3]. The reason for the sudden decrease in light emission is unclear. However, it may suggest that appreciable beam radial expansion seemed to occur due to an increase in the negative charge density of the beam. After the point of beam spreading, the beam evolved into a hollow cylindrical shell structure which propagated parallel to the local magnetic field. The vehicle electric potential induced by these electron beam firings was normally a few volts to a few tens of volts with a beam energy of 1 keV [2].

Space Experiments with Particle Accelerators (SEPAC) during the Spacelab 1 mission indicated that the electron beam injection had charged the spacecraft to a potential as high as the beam energy, which was 5 keV [5]. Because the ambient plasma cannot neutralize

the electron beam and the spacecraft, the net beam charge and the spacecraft charging are important in this case in determining beam propagation and expansion.

In laboratory experiments, Kellogg et al. [4] studied radial expansion of electron beams injected into a background plasma and neutral gas. When the electron gun was grounded, the envelope of the beam was twice the beam electron gyroridus radius ρ_e where $\rho_e = v_b/\Omega_{ce}$ for cross-field injection. For the aligned beam the radius of the envelope was $r_b \approx 0.25\rho_e$. However, when the electron gun was allowed to float and no background plasma was present, the electron beam appeared to have a diameter approximately twice the beam electron gyroradius. In these cases the gun potential rose to the electron beam accelerator potential. Therefore, charging seems to play an important role in the beam radial expansion.

Several two-dimensional simulations show that high density electron beams can propagate in the plasma because the net beam charge has caused the beam to expand radially and reduced the beam density [9–12]. In particular, Winglee and Pritchett [11] have simulated cross-field and parallel electron beam injection, concentrating on moderate spacecraft charging. For cross-field injection the beam is found to form a hollow cylinder of radius approximately equal to the beam gyroradius and width of about $2\lambda_{Db}$ where $\lambda_{Db} = v_b/\omega_b$. The beam width is believed to be caused by repulsive forces associated with a net negative charge within the beam. For parallel injection slower beam electrons are overtaken, causing a net repulsive force to push the beam electrons outward to a cylinder thickness comparable to the cross-field injection case. The maximum perpendicular velocity was found to be comparable to the parallel beam velocity.

Analytic calculations [13] for electron beams injected parallel to magnetic field lines

have shown that space charge effects play an important role during the initial phase of beam expansion. Furthermore, the magnetic field determines the beam radius and beam density. However, the calculations did not take into account any possible beam instabilities.

In this paper we study radial expansion of electron beams injected parallel to the magnetic field. We have used a two-dimensional electrostatic particle code to simulate the electron beam injection from an isolated finite equipotential conductor into a plasma. In contrast to Winglee and Prichett [12], we concentrate on cases of high spacecraft charging, which are more applicable to SEPAC electron beam firings. It is shown that radial expansion is significant. We also surveyed the simulation results to determine the dependence of the beam expansion on the background magnetic field, beam density, and beam velocity.

SIMULATION MODEL

To study electron beam injection from a conductor, we modified a 2-D particle-in-cell code, DARWIN, which was originally developed at Los Alamos National Laboratory [14]. Here we present the simulation results in the electrostatic limit. Realistic modeling of beam injection from a spacecraft required injecting an electron beam from a finite isolated conductor. The simulation geometry is shown in Figure 1.

Particles are injected from the spacecraft surface in the simulation box every time step. The number of injected electrons per time step per cell is $N_c(e/q_e)(n_b/n_c)v_b\Delta t$ where N_c is the number of ambient electrons per cell, Δt is the simulation time step, n_b/n_c is the ratio of the beam density to ambient density, and e/q_e is the ratio of the ambient electron charge to the beam electron charge. The beam electrons have fractional charge and mass, which allows

an increase in the number injected per time step. This larger number for the same beam density reduces numerical noise. These particles are placed in the simulation box at positions $x = Rv_b\Delta t$ where x is the distance from the conductor surface, v_b is the injection velocity, and R is a random number between 0 and 1 for each injected particle. This method tends to fill in the fan between $x = 0$ and $x = v_b\Delta t$. The injected particles are randomly distributed across the beam in the y direction. All particles which strike the spacecraft surface are absorbed and their charge is accumulated.

Treating the spacecraft surface as a finite isolated equipotential conductor in an ambient plasma was accomplished by using the capacity matrix method [11,15]. The capacity matrix relates the charge on each grid point on the spacecraft to the corresponding potential.

$$q_i = \sum_j C_{ij}\Phi_j \tag{1}$$

where C_{ij} is the capacity matrix, Φ_j is the spacecraft potential, and the sum j is over every grid point on the spacecraft. The capacity matrix is found by placing a unit charge on one point of the spacecraft surface with all other points zero and then solving for the potential. The values of the potential at each point on the spacecraft represent one column in the inverse capacity matrix $A = C^{-1}$. Repeating the process for each node then generates the full inverse matrix. The capacity matrix is obtained from the inverse of this matrix. This process is carried out only once at the beginning of the program. During the program the code first solves Poisson's equation for the electric potential Φ_0 with charge evenly distributed on the spacecraft surface. Second, it uses the capacity matrix of the conductor to redistribute the

charge and maintain the spacecraft surface at an equipotential using the formulae:

$$\Delta q_i = \sum_j C_{ij}(\Phi_{eq} - \Phi_{0j}) \tag{2}$$

$$\Phi_{eq} = \sum_{ij} C_{ij} / \sum_{ij} C_{ij} \tag{3}$$

where Δq_i is the charge that is added to each grid point on the spacecraft. Using the redistributed charge density, the code again solves Poisson's equation for the electric potential of the spacecraft.

We use a periodic boundary condition for the lower boundary at $y = 0$ and the upper boundary at $y = L_y$ where L_y is the simulation length in the y direction. The electrostatic potential at $x = 0$, $\phi(x = 0, y)$, is constant. We assume the potential is zero at the right boundary at $x = L_x$ where L_x is the simulation length in the x direction. The right boundary condition approximates the potential at infinity.

Ambient ions and electrons are initialized uniformly in the system with a uniform magnetic field in the x direction. Both the ambient ions and electrons have Maxwellian velocity distributions with the same temperature, $T_e = T_i$ where T_e and T_i are the electron and ion temperatures, respectively. At the right and left boundary, the code specularly reflects all particles.

SIMULATION RESULTS

The simulation uses a $512\Delta \times 128\Delta$ grid in the x and y directions, respectively. The spacecraft is represented by a rectangular box centered on $x = 102\Delta$ and $y = 64\Delta$ with size $4\Delta \times 32\Delta$ in the x and y directions, respectively. The grid size, Δ, equals the Debye length of

the ambient electrons defined as $\lambda_d = a_c/\omega_{pe}$ where $a_c = (2T_e/m_e)^{1/2}$ is the thermal velocity of the ambient electrons and ω_{pe} is the ambient electron plasma frequency. We choose the ion to electron mass ratio to be 100, and $a_c = 0.001c$ where c is the speed of light, a unit of the simulation. We use a reference electron gyrofrequency Ω_{ce} of $0.25\omega_{pe}$, which is close to the ionospheric value of $0.3\omega_{pe}$. The simulations use a time step $\Delta t = 0.05\omega_{pe}^{-1}$ and 131,072 particles for the ambient plasma. For the reference case the electron beam has a width of 4Δ, an injection velocity of $v_b = 10a_c$ along the x axis, zero initial thermal velocity, and a density ratio of $n_b/n_c = 10$.

Figures 2-4 show results of electron beam injection for the reference parameters. The phase space plot $x - v_x$ at $\omega_{pe}t = 30$ in Figure 2a indicates that the point at which beam electrons are stopped (stagnation point) is very close to the conductor surface. Due to the high beam density the spacecraft becomes positively charged, causing the beam electrons to be rapidly drawn back to the spacecraft surface. The average electrostatic potential of the spacecraft in this case is $\approx$ 94% of the beam energy. Some electrons at the front of the beam are accelerated to velocities higher than the original beam velocity. This is due to the bunching of beam electrons behind the beam head. Also some returning beam electrons overshoot the spacecraft and are drawn back on the wake side. The configuration space plot given in Figure 2b shows that the electron beam expands radially. Figure 3a shows a contour plot of the beam density where the contour line delineates the beam edge. From this plot the beam radius is approximately $r_b = 40\Delta$. The beam electron gyroradius $\rho_e = v_b/\Omega_{ce}$ is also 40Δ where v_b is the initial beam velocity. It is apparent from earlier configuration space plots that the maximum beam expansion occurs near the stagnation point, which is very

close to the spacecraft surface. The highest beam density is at the stagnation point of the beam (Figure 3b). This is in agreement with analytical results for one-dimensional electron beam injection into a vacuum [16]. Physically, the high density at the stagnation point is understood in an approximate sense by the conservation of flux $n_b v_b$. At the stagnation point, where the average beam velocity is smallest, the density should be highest assuming substantial expansion of the beam has not occurred.

Figure 4a and 4b show that the maximum transverse electric field E_y and the maximum longitudinal electric field E_x occur where the beam density is highest. The transverse velocities to which the beam electrons are accelerated depend on the time spent in the stagnation region, where the transverse electric fields are largest. This can be estimated from the width of the transverse electric field region, approximately 8Δ, and the initial beam velocity. From these values it is apparent that the beam particles can be accelerated to 75% of the initial beam velocity. In general beam electrons travel through the stagnation region with velocities lower than the initial beam velocity. So they spend more time in the stagnation region and are accelerated to higher velocities. After the stagnation region the transverse electric field E_y is smaller (Figure 4a) and the average beam velocity is higher (Figure 2a). Therefore, the beam electrons receive their largest tranverse kick very close to the spacecraft and experience smaller transverse impulses from that point on.

Variation with Magnetic Field Strength

Figure 5 shows beam density plots at $\omega_{pe}t = 30$ where the contour lines indicate the beam envelope. The magnetic field Ω_{ce}/ω_{pe} is 0.25, 0.5, and 1.0 down the page with all other

parameters fixed. Note that the maximum beam radius decreases with increasing magnetic field. The ratio of the maximum beam radius to the electron gyroradius r_b/ρ_e is approximately 1 for each of these cases. This indicates that independent of the magnetic field the beam electrons receive the same transverse kick and expand to ρ_e in the range of ionospheric magnetic field values. In Figure 5c, where $\Omega_{ce}/\omega_{pe} = 1.0$, no beam electrons are in the wake region of the spacecraft. The maximum width beam electrons achieve, $2\rho_e$, is smaller than the spacecraft width. So all returning beam electrons strike the spacecraft surface.

Variation with Beam Density

Figure 6 shows simulation results at $\omega_{pe}t = 30$ varying the beam to ambient plasma density ratio n_b/n_c from 1 to 20 for the cases of $\Omega_{ce}/\omega_{pe} = 0.25$ (solid line) and 0.5 (dotted line). The ratio r_b/ρ_e is between 0.725 for $n_b/n_c = 1$ and 1.3 for $n_b/n_c = 20$. The maximum beam radius gradually increases with beam density. This indicates that the transverse kick that the beam electrons receive gradually increases with beam density. The relative magnitude of the transverse kick can be obtained from the average velocity of the beam electrons through the stagnation region. The average velocity gives a rough idea of the time that the beam electrons are accelerated by the transverse electric fields E_y in the stagnation region. Figure 7 shows the average velocity of beam electrons at the stagnation point versus beam density for $\Omega_{ce}/\omega_{pe} = 0.25$ (solid line) and 0.5 (dotted line) at $\omega_{pe}t = 30$. The velocity is averaged across the beam and the stagnation point is taken to be the point where the longitudinal electric field E_x is a maximum. The average velocity decreases with increasing beam density for both values of magnetic field. This indicates that beam electrons spend more time in the

stagnation region for higher density beams and are, therefore, accelerated to higher transverse velocities. The ratio of the electron beam Debye length λ_{Db} to the ambient electron Debye length λ_d, which is

$$\frac{\lambda_{Db}}{\lambda_d} = (\frac{v_b}{a_c})(\frac{n_c}{n_b})^{1/2}, \tag{4}$$

gives an understanding of this velocity trend. The electron beam Debye length is an indication of the charge separation distance between the spacecraft and the beam stagnation point. The ambient electron Debye length indicates the distance above which ambient electrons neutralize excess charge. As this ratio decreases the beam electrons feel the Coulombic potential of the spacecraft more since ambient electrons have a harder time shielding the effects of the retarding potential drop. Therefore, the beam electrons travel with lower velocities. This ratio decreases with increasing beam density n_b as $n_b^{-1/2}$ following the trend of the average velocity in Figure 7.

Variation with Beam Velocity

Figure 8 shows the beam radius normalized to the electron gyroradius r_b/ρ_e as a function of initial injection velocity v_b at $\omega_{pe}t = 30$. The injection velocity v_b/a_c where a_c is the ambient electron thermal velocity is varied between 2.5 and 20.0. All other parameters are the same as in the reference case. The radial expansion is largest for small velocity injection and smallest for high velocity injection. The relative magnitude of the transverse kick can again be inferred from the average velocity of the beam electrons through the stagnation region. Figure 9 shows the average velocity of beam electrons at the stagnation point versus initial beam injection

velocity at $\omega_{pe}t = 30$. The average velocity increases with the initial beam injection velocity. Beam electrons spend more time in the stagnation region for lower injection velocities and are, therefore, accelerated to higher relative transverse velocities. This velocity trend can also be interpreted from the ratio of the beam electron Debye length to the ambient electron Debye length. This ratio increases linearly with the initial beam injection velocity. As the beam injection velocity increases, the ambient electrons are more able to shield excess charge buildup over the beam electron Debye length. Therefore, the beam electrons travel with higher velocities through the stagnation region, which is in agreement with Figure 9.

DISCUSSION AND CONCLUSION

We have examined the radial expansion properties of a nonrelativistic electron beam injected along magnetic field lines into a background plasma. We have concentrated on high beam current cases where spacecraft charging is significant. In our reference case with $n_b/n_c = 10$ and $v_b/a_c = 10$, the beam expanded to twice the beam electron gyroradius ρ_b. The beam electrons receive a large transverse kick from beam electrons which have built up at the stagnation point. This kick, which occurs very close to the injection point, determines the beam envelope from that point on. We have found that the transverse energization of the beam electrons is independent of the strength of the magnetic field for values between $\Omega_{ce}/\omega_{pe} = 0.25$ and 1. The beam envelope is twice the beam electron gyroradius ρ_e. We have also found that the beam envelope increases with beam density. The average velocity of beam electrons through the stagnation region decreases with increasing beam density. The average velocity indicates the time beam electrons spend in the stagnation region and, therefore, how

long beam electrons are accelerated by the transverse electric fields. The final transverse velocity of the beam electrons and, thus, the beam envelope increases with beam density. Variation of the initial beam injection velocity indicates that the beam envelope decreases with increasing beam injection velocity. The average velocity of beam electrons through the stagnation region increases with beam injection velocity. Therefore, beam electrons with high injection velocity are accelerated to lower relative transverse velocities than beam electrons with low injection velocities. The ratio of λ_{Db}/λ_d, which is an indication of how well beam electrons are shielded from the charged spacecraft surface by the ambient electrons, can be used to explain the dependence of beam radius on beam density and beam injection velocity. This dependence is evident from Figure 7 where the average beam velocity at the stagnation point drops off approximately as $n_b^{-1/2}$ and from Figure 9 where the average velocity increases almost linearly with beam injection velocity v_b.

The spacecraft potential energy in each of these runs varied between 60% and 100% of the beam energy except for the cases of low beam density. These results are most applicable to the SEPAC electron beam injection experiments where the Shuttle was charged to the beam energy. In future work we will address the problem of beam radial expansion when collisional ionizations of neutrals by the beam electrons is taken into account.

ACKNOWLEDGMENTS

The authors would like to thank R. M. Winglee for collaboration on simulation techniques. The work was supported by NASA contract NAGW–1231 and by Lewis Research Center through NASA Contract Nas8-32488. The particle simulations were performed on the CRAY-YMP at NASA Ames Research Center.

REFERENCES

[1] B. Grandal, ed., " Artificial Particle Beams in Space Plasma Studies", Plenum, New York, 1982.

[2] P. M. Banks, W. J. Raitt, A. B. White, R. I. Bush, and P. R. Williamson, "Results from the vehicle charging and potential experiment on STS-3", *J. Spacecr. Rockets*, vol. 24, p. 138, 1987.

[3] P. M. Banks and W. J. Raitt, "Observations of electron beam structure in space experiments", *J. Geophys. Res.*, vol. 93, p. 5811, 1988.

[4] P. J. Kellogg, H. R. Anderson, W. Bernstein, T. J. Hallinan, H. R. Holzworth, R. J. Jost, H. Leinbach, and E. P. Szuszuczewicz, "Laboratory simulation of injection particle beams in the ionosphere", *Artificial Particle Beams in Space Plasma Studies*, edited by Bjorn Grandel, 1982, pp. 289-329.

[5] S. Sasaki, N. Kawashima, K. Kuriki, M. Yanagisawa, and T. Obayashi, "Vehicle charging observed in SEPAC Spacelab-1 experiment", *J. Spacecr. Rockets*, vol. 23, no. 2, p. 129, 1986.

[6] Y. Omura, and H. Matsumoto, "Computer simulations of beam injection experiments for SEPAC/Spacelab 1 mission", *Radio Sci.*, vol. 19, no. 2, p. 496, 1984.

[7] P. L. Pritchett, and R. M. Winglee, "The plasma environment during particle beam injection into space plasmas, 1, electron beams", *J. Geophys. Res.*, vol. 92, no. A7, p. 7673, 1987.

[8] H. Okuda, and J. R. Kan, "Injection of an electron beam into a plasma and spacecraft charging", *Phys. Fluids*, vol. 30, No. 1, p. 209, 1987.

[9] R. M. Winglee, and P. L. Pritchett, "Space charge effects during the injection of dense electron beams into space plasmas", *J. Geophys. Res.*, vol. 92, no. A6, p. 6114, 1987.

[10] H. Okuda, and J. Berchem, "Injection and propagation of a nonrelativistic electron beam and spacecraft charging", *J. Geophys. Res.*, vol. 93, no. A1, p. 175, 1988.

[11] R. M. Winglee, and P. L. Pritchett, "Comparative study of cross-field and field-aligned electron beams in active experiments", *J. Geophys. Res.*, vol. 93, no. A6, p5823, 1988.

[12] C. S. Lin and J. K. Koga, "Spacecraft charging potential during electron-beam injections into space plasmas", *IEEE Trans. Plasma Sci.*, vol. 17, no. 2, p. 205, 1989.

[13] R. Gendrin, "Initial expansion phase of artificially injected electron beam", *Planet. Space Sci.*, vol. 22, p. 633, 1974.

[14] C. W. Nielson, H. R. Lewis, "Particle simulation techniques in the nonradiative limit", *Methods Comput. Phys.* vol. 16, p. 367, 1976.

[15] R. W. Hockney and J. W. Eastwood, "Computer simulation using particles", McGraw-Hill, New York, 1981.

[16] D. E. Parks, A. R. Wilson, and I. Katz, "Monode plasma sheath dynamics", *IEEE trans. Nucl. Sci.*, vol. NS-22, no. 6, p. 2368, 1975.

FIGURE CAPTIONS

Fig. 1. Simulation configuration.

Fig. 2. Results of simulation for $n_b/n_c = 10$ and $v_b/a_c = 10$ at $\omega_{pe}t = 30$. (a) The beam electron phase space in the x-v_x plane and (b) the positions of beam electrons in the x-y plane. The position is normalized by the Debye length and the velocity is normalized by the initial beam injection velocity.

Fig. 3. Density plots of beam electrons at $\omega_{pe}t = 30$ for $n_b/n_c = 10$ and $v_b/a_c = 10$. (a) Contour lines delineate beam envelope. (b) Profile of beam density along beam showing maximum density close to spacecraft surface.

Fig. 4. Profiles of maximum field quantities across beam at $\omega_{pe}t = 30$. (a) Maximum transverse electric field E_y and (b) maximum longitudinal electric field E_x.

Fig. 5. Density plots of beam electrons at $\omega_{pe}t = 30$ for $n_b/n_c = 10$ and $v_b/a_c = 10$. Contour lines delineate beam envelope. Ω_{ce}/ω_{pe} = (a) 0.25, (b) 0.5, and (c) 1.0

Fig. 6. Electron beam envelope radius r_b/ρ_e versus n_b/n_c at $\omega_{pe} = 30$ for $v_b/a_c = 10$.

Fig. 7. Average velocity v_x at the stagnation point normalized to ambient electron thermal velocity a_c versus n_b/n_c at $\omega_{pe} = 30$ for $v_b/a_c = 10$.

Fig. 8. Electron beam envelope radius r_b/ρ_e versus initial beam injection velocity v_b/a_c at $\omega_{pe} = 30$ for $n_b/n_c = 10$.

Fig. 9. Absolute value of average velcity v_x at the stagnation point normalized to ambient electron thermal velocity a_c versus initial injection velocity v_b/a_c at $\omega_{pe} = 30$ for $n_b/n_c = 10$.

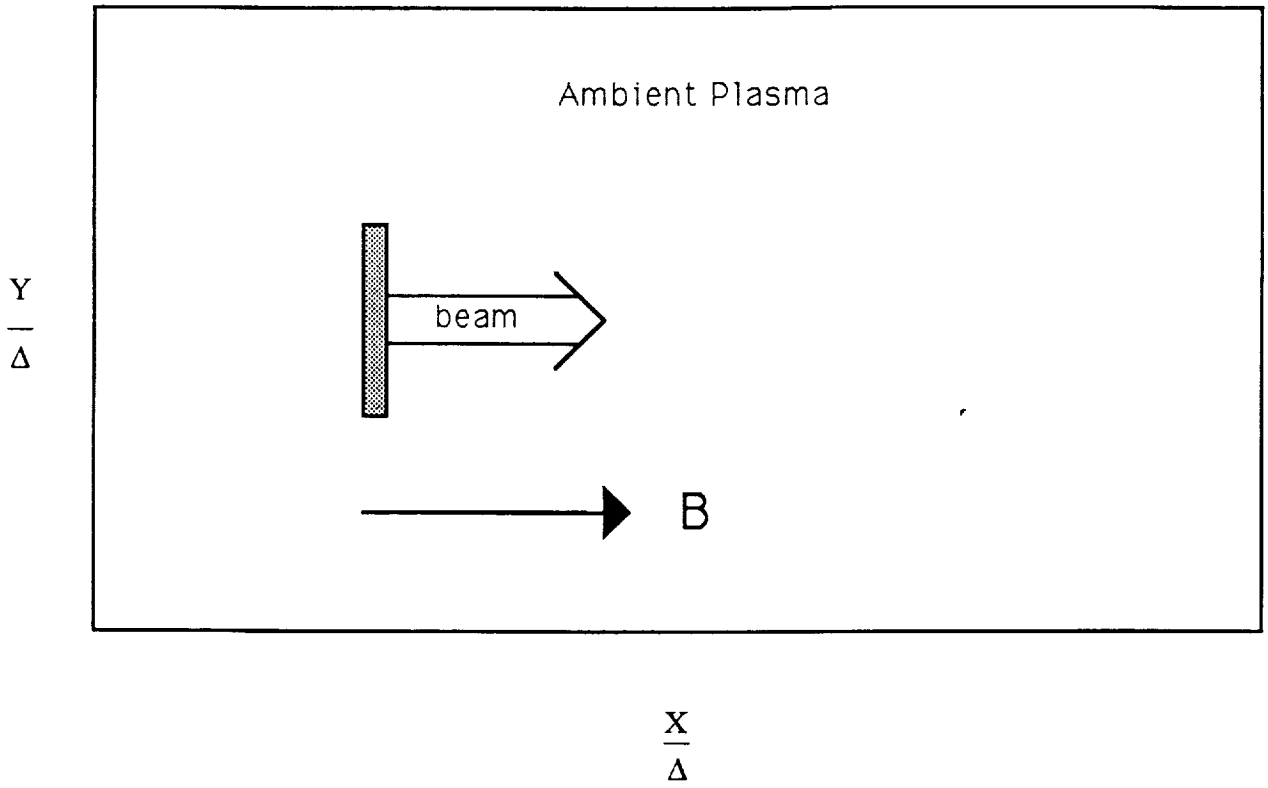

Figure 1

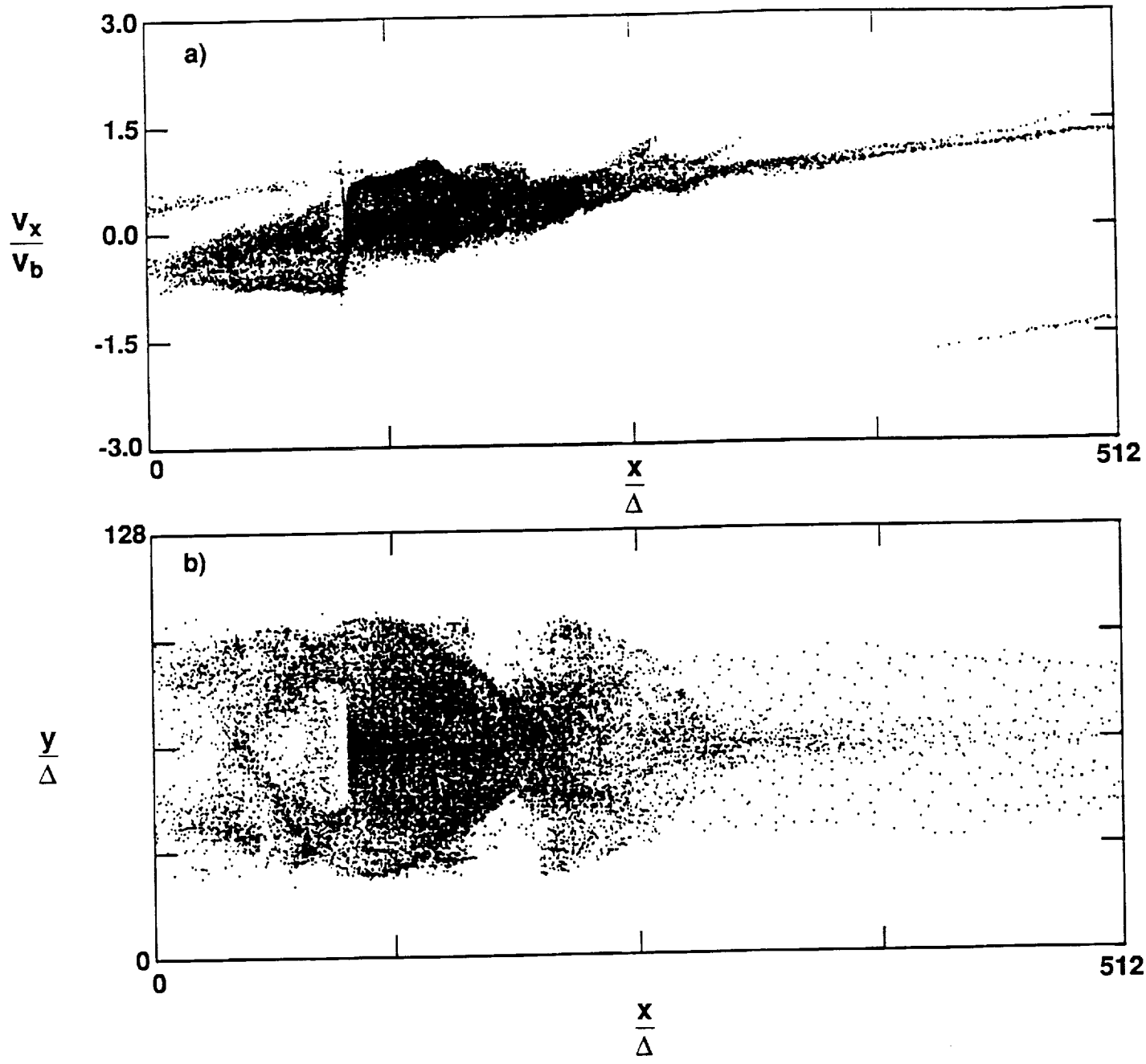
3.0
a)
1.5
$\frac{V_x}{V_b}$
0.0
-1.5
-3.0
0
512
$\frac{x}{\Delta}$
128
b)
$\frac{y}{\Delta}$
0
0
512
$\frac{x}{\Delta}$

Figure 2

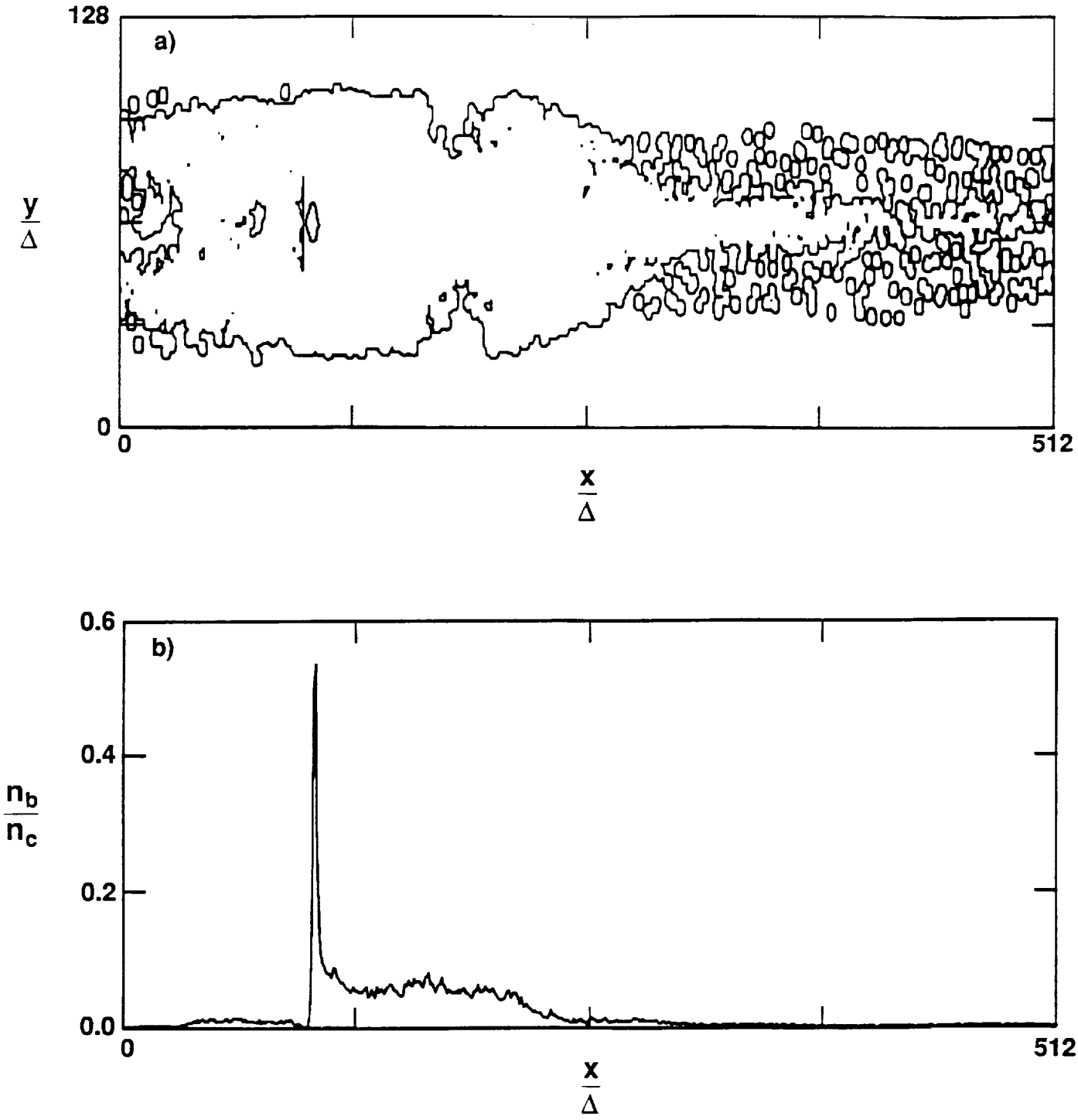

Figure 3

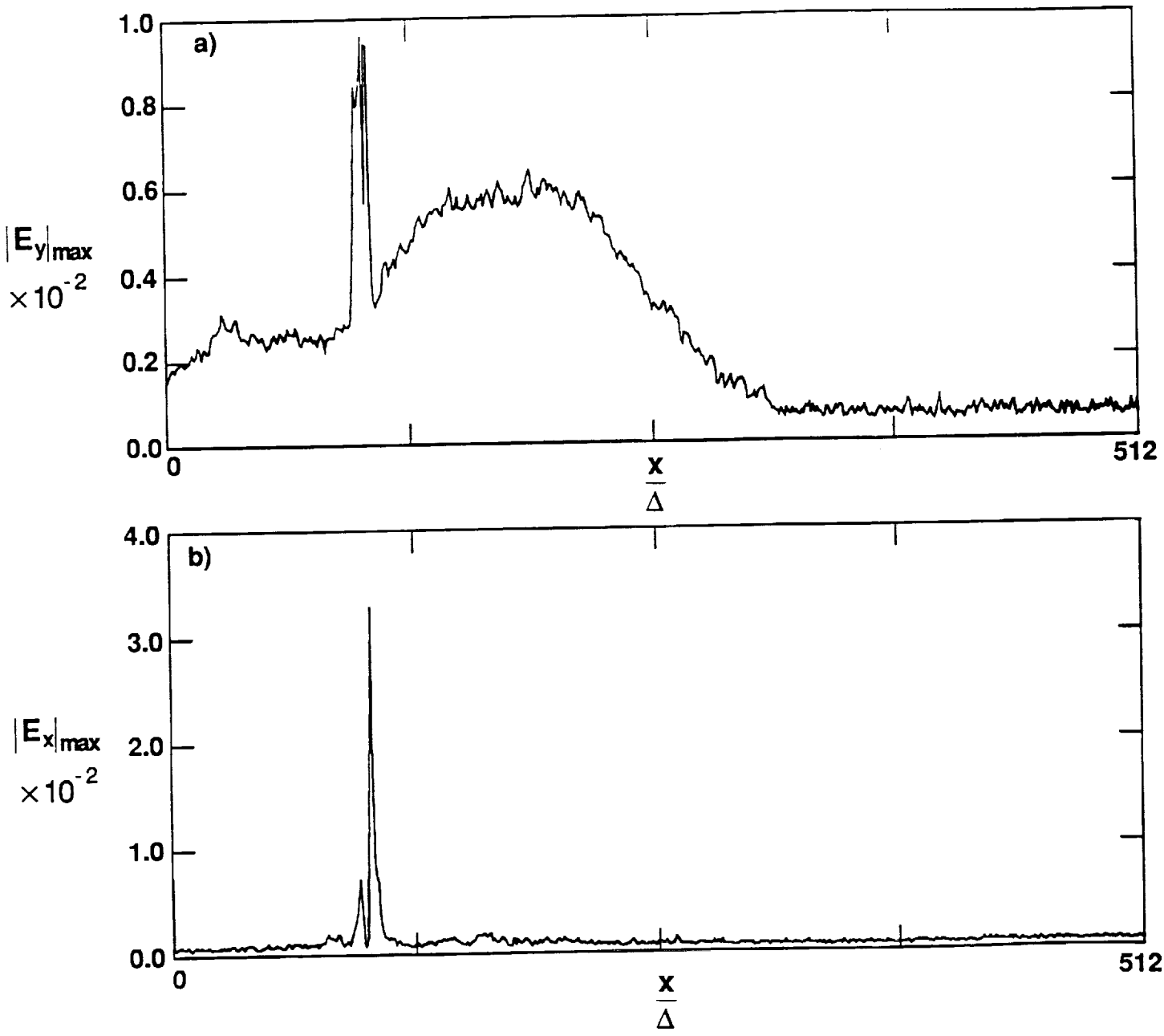
a)
1.0
0.8
0.6
0.4
0.2
0.0
$|E_y|_{max}$
$\times 10^{-2}$
0
512
X
Δ
b)
4.0
3.0
2.0
1.0
0.0
$|E_x|_{max}$
$\times 10^{-2}$
0
512
X
Δ

Figure 4

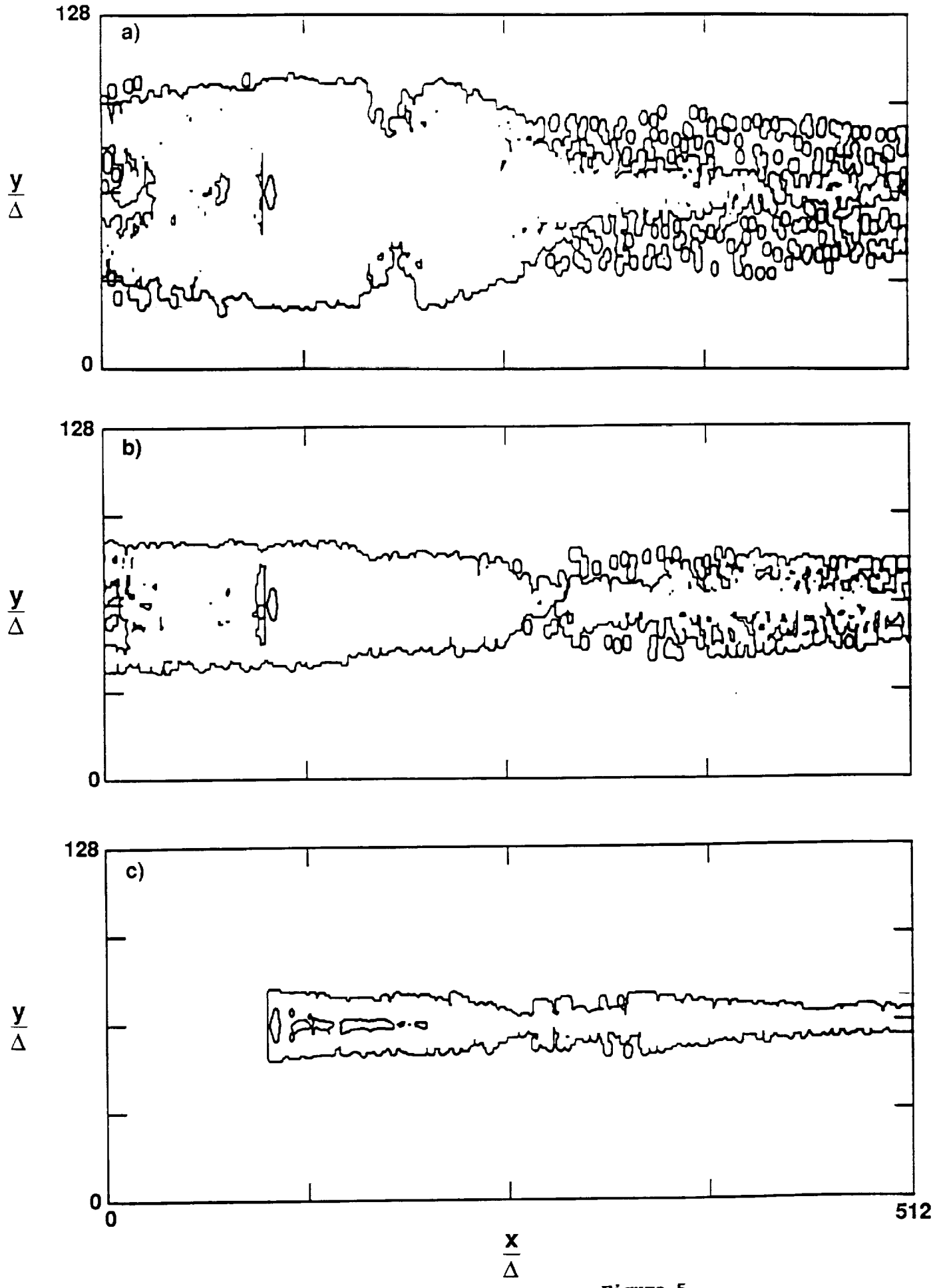

Figure 5

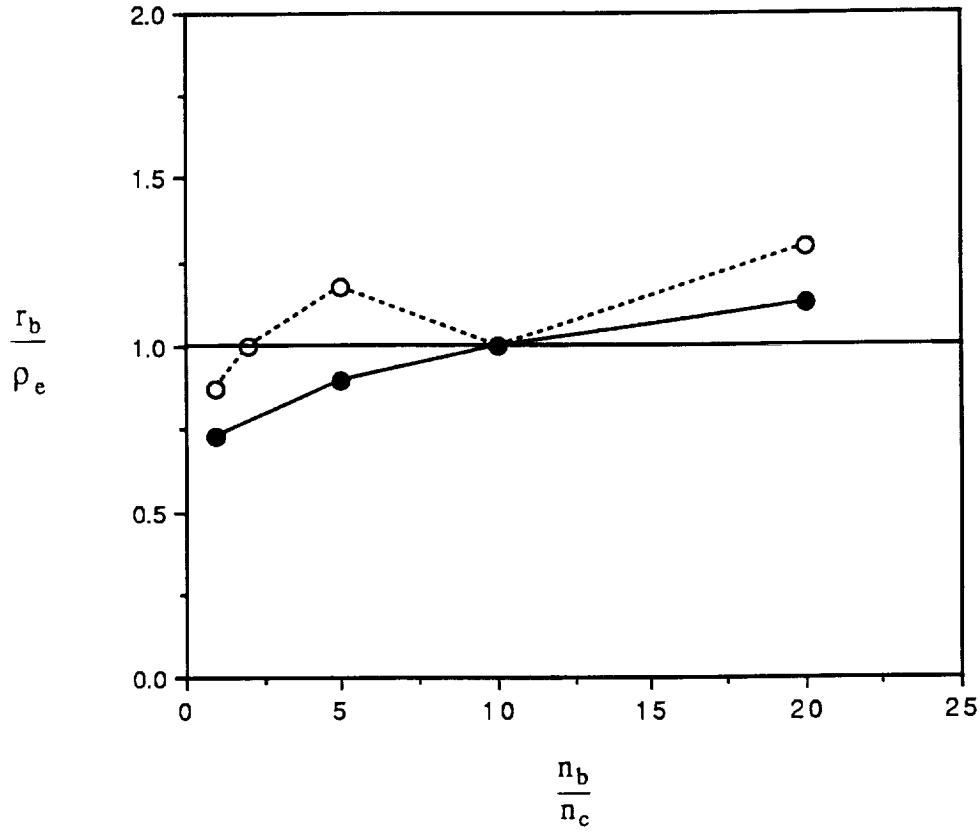

Figure 6

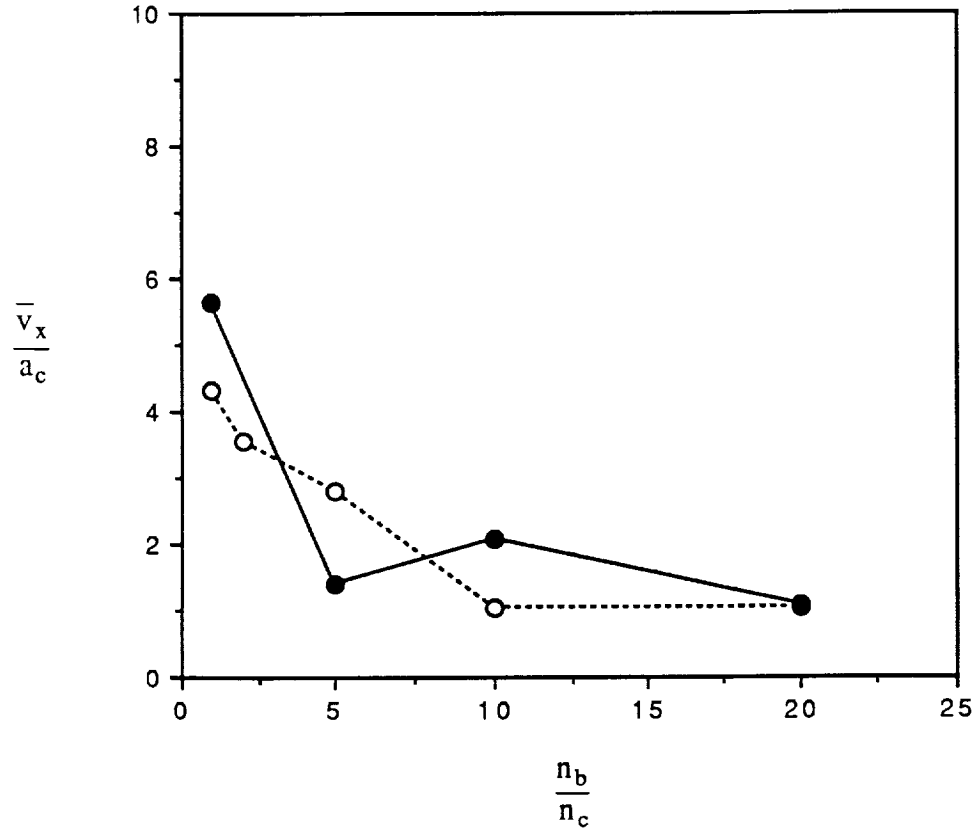

Figure 7

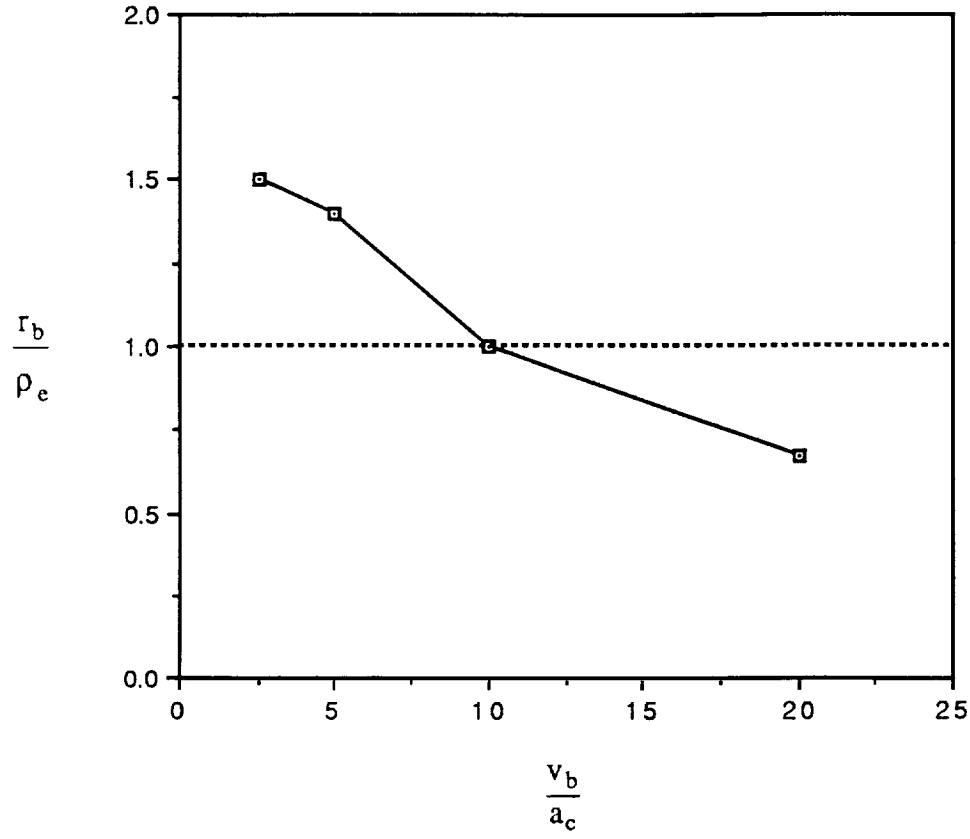

Figure 8

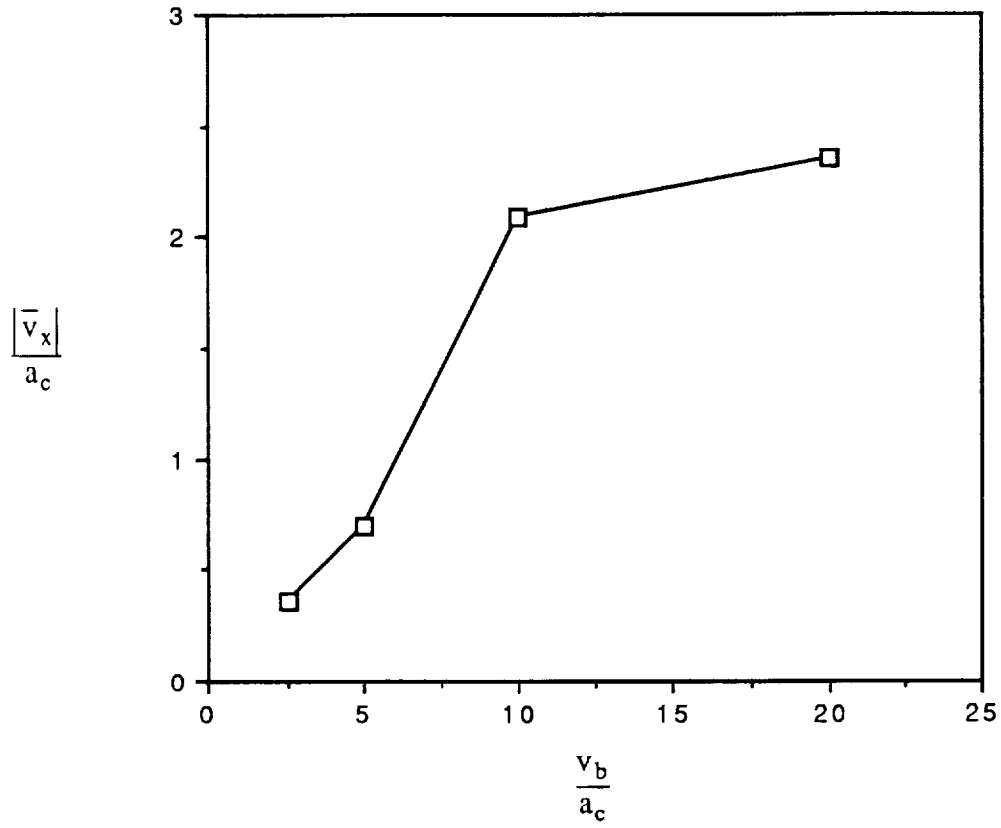

Figure 9